Optical Microscopy of Growing Insulin Amyloid Spherulites on Surfaces In Vitro

Salman S. Rogers,* Mark R. H. Krebs,* Elizabeth H. C. Bromley,* Erik van der Linden,† and Athene M. Donald*
*Cambridge University, Cambridge, United Kingdom; and †Wageningen University, Wageningen, The Netherlands

ABSTRACT Amyloid fibrils are often found arranged into large ordered spheroid structures, known as spherulites, occurring in vivo and in vitro. The spherulites are predominantly composed of radially ordered amyloid fibrils, which self-assemble from protein in solution. We have observed and measured amyloid spherulites forming from heat-treated solutions of bovine insulin at low pH. The spherulites form in large numbers as semispherical dome-shaped objects on the cell surfaces, showing that surface defects or impurities, or the substrates themselves, can provide good nucleation sites for their formation. Using optical microscopy, we have measured the growth of individual spherulites as a function of time and in various conditions. There is a lag time before nucleation of the spherulites. Once they have nucleated, they grow, each with a radius increasing linearly, or faster than linearly, with time. Remarkably, this growth period has a sudden end, at which all spherulites in the system suddenly stop growing. A model of spherulite formation based on the polymerization of oriented fibrils around a nucleus, from a precursor in solution, quantitatively accounts for the observed growth kinetics. Seeding of native insulin solutions with preformed spherulites led to the preformed spherulites growing without a lag time. This seeding behavior is evidence that the fibrils in the spherulites assemble from small protein species rather than fibrils. The density of the spherulites was also measured and found to be constant with respect to radius, indicating that the space fills as the spherulite grows.

INTRODUCTION

A wide range of proteins is known to misfold and aggregate in mildly denaturing conditions into large polymeric structures known as amyloid fibrils. These fibrils are found in a range of degenerative diseases, such as Alzheimer's disease, Parkinson's disease, type II diabetes, prion diseases, senile systemic amyloidosis, and Huntingdon's disease. The fibrils can also be formed in vitro, from proteins associated with a disease, as well as proteins associated with none (1).

Amyloid fibrils have been found to be based on a common structure, consisting of continuous intermolecular β-sheets which run along the fibril axis, such that the individual β-strands are perpendicular to the fibril axis (2). This common structural motif, based only on the peptide backbone, as well as the observation that a wide variety of proteins forms these fibrils, suggests that amyloid fibrils are a generic form of protein assembly structure (3). The fibrils tend to be long (>1 μm) and unbranched, with diameters typically between 6 and 12 nm (4).

In the different amyloid diseases, the fibrils are deposited in various forms. In a form identified in Alzheimer's disease and Downs' syndrome, they are found in birefringent spherical plaques (5). The birefringence of the plaques shows that the material of which they are composed is anisotropic, and ordered in a spherically symmetric way. In some diseases, amyloid deposits occur in vast quantities but it is still generally unknown what role, if any, the fibrils and plaques may have in each disease.

Large spherical ordered assemblies of amyloid fibrils have been observed in several other systems in vivo and in vitro (6–20), and are described by various names. Here we term them *spherulites*, by analogy to the similar, ordered structures formed by crystallizing polymers (21–23).

Bovine insulin is a small protein whose ability to form fibrillar structures and spherulites has been known for almost 60 years (7). The fibrils are characterized by the same features as other amyloid fibrils (24,25). Some details of the molecular structure have been determined, using data from cryoelectron microscopy (26). Each fibril contains a number of protofilaments twisted together, each protofilament being a linear chain of insulin molecules (26). The spherulites have been found to be structurally similar to the wide range of amyloid spherulite structures described above (6,27,28).

Krebs et al. (6,27) suggested that the spherulites are composed of amyloid fibrils that grow outwards from a core, which may be a protein aggregate without amyloid structure. Spherulite cores could be observed that were in contrast with the surrounding material because of their lack of directional order and lack of affinity to amyloid-specific dyes (6). Comparing the onset of spherulite formation and the formation of fibrils dispersed in the solution led to evidence that the growing spherulites do not assemble from the dispersed fibrils, but more likely from a small precursor species—either insulin monomers or small oligomers in solution. Therefore, assembly of proteins into spherulites may proceed along a separate (though not necessarily dissimilar) pathway to assembly of proteins into dispersed fibrils. Insulin spherulites are formed in large quantities in solutions of bovine insulin, at pH 2 or lower, while under prolonged heating at temperatures of 65°C or higher. Under these conditions,

Submitted August 15, 2005, and accepted for publication October 4, 2005.
Address reprint requests to A. M. Donald, E-mail: amd3@cam.ac.uk.

0006-3495/06/02/1043/12 $2.00
doi: 10.1529/biophysj.105.072660

a high proportion (~90–95%) of insulin is converted to spherulites and dispersed fibrils, with the remainder in the form of insulin monomers or small oligomers (6). Therefore, it seems that the reaction of insulin to form spherulites and fibrils is limited by depletion of the precursor.

In this article, we observe bovine insulin spherulites forming on cell surfaces using differential interference contrast (DIC) contrast optical microscopy. The resulting timelapse video images are used to track the growth of individual spherulites with time, in various conditions. These measurements of growth are complemented with other images and measurements to provide insights into the structure, formation mechanism, and growth kinetics of the spherulites. We propose a growth model, limited by the rates of fibril elongation and precursor diffusion to account for our measurements. Seeding of native insulin solutions with preformed spherulites and other nucleation effects are also observed.

EXPERIMENTAL PROCEDURES

Sample preparation

Bovine insulin and all other chemicals were of analytical grade or better, and were obtained from Sigma-Aldrich, Gillingham, UK and used without further purification. Insulin solutions of concentration 5.0 mg/ml were made by weighing the dry powder and dissolving in Milli-Q deionized water adjusted to pH 1.50 with HCl (Millipore, Billerica, MA). The insulin solutions were then readjusted to pH 1.50 with concentrated HCl. These solutions were filtered with a 0.45-μm Millipore protein filter to remove dust and aggregated or undissolved protein, after which they were vacuum-degassed. They were then put into glass cavity slides and sealed with coverslips. These slides and coverslips had been previously cleaned with concentrated hydrochloric/nitric acids to remove any traces of organic residues on their surfaces. In experiments where samples were compared under different conditions, the same insulin stock solution was used for each to ensure that the pH, insulin concentration, and trace impurities were the same for all samples.

Polystyrene-coated surfaces were also used for some experiments: a cavity slide and coverslip were solution-coated with polystyrene by dipping in a polystyrene/toluene solution and allowing to dry.

Optical microscopy of spherulite formation

Each sample was placed on a Linkam hot-stage set to temperatures of 65–75°C under a Zeiss Axioplan optical microscope (Carl Zeiss, Welwyn Garden City, UK) in DIC mode, at 100× magnification. The microscope was focused on the lower surface of the cell to view the spherulites which form immobilized on the surface. Digital images were taken, and timelapse videos composed. Distances in the image plane were calibrated by imaging a 100-μm scale bar, resulting in a resolution of 1.295 μm/pixel.

Measurement of spherulite sizes

Since most spherulites have an approximately circular shape on the micrographs, a radius of each could be measured. Spherulites which were out-of-focus or deviated significantly from a circular shape, especially where two or more spherulites were joined together, were excluded. For each spherulite, the radius was measured from a manually chosen center, to the outside edge, defined by its sharp increase in brightness on the DIC images. A MatLab (The MathWorks, Natick, MA) script was written to find this edge. Due to the irregularities in the shape of the spherulites, a typical radial error of ± 5 μm is estimated.

Laser scanning confocal microscopy

Confocal microscopy allowed vertical cross-sectional images to be made of spherulites bound to a surface. A Zeiss LSM510 confocal microscope was used (Carl Zeiss). A coverslip coated with insulin spherulites was submerged in a solution of the amyloid-specific dye, thioflavin-T, of concentration 0.1 mg/ml at pH 1.5, and sealed with a cavity slide. An optical magnification of 500× and pinhole size of 50 μm were used. The dye was excited with the 458-nm line of an Argon ion laser. By scanning through the spherulite in three dimensions, cross-sections of the spherulite could be captured.

Seeding of insulin solutions with preformed spherulites

An insulin solution of concentration 5.0 mg/ml at pH 1.5 was prepared as in Sample Preparation, above, and heated at 70°C in an Eppendorf tube for 2 h, forming many unattached spherulites. These spherulites were rinsed as follows: a small amount (200 μl) of the solution containing spherulites was transferred to a dilute HCl solution at pH 1.5 (1 ml), stirred and mildly centrifuged to sediment the spherulites. The excess HCl solution was decanted and replaced with a fresh pH 1.5 HCl solution.

Ten-microliter aliquots of the rinsed spherulite solution, containing small numbers of preformed spherulites, were added to fresh solutions of insulin of variable concentration 0.2–5.0 mg/ml, at pH 1.5, in cavity slide cells. Each sample was heated at 70°C (as in Optical Microscopy of Spherulite Formation, above) to measure the growth of the preformed spherulites in fresh insulin solutions.

Spherulite density measurements

An insulin solution, prepared as described above, was heated at 70°C for 2 h in an Eppendorf tube. The unattached spherulites were separated from the solution by mild centrifugation, rinsed and transferred to a solution of HCl in a rectangular cuvette cell with the same ionic conditions as those in which they were prepared (pH 1.5). The cuvette was mounted vertically and imaged with the telecentric zoom microscope of an FTA200 system (First Ten Angtroms, Portsmouth, VA), at maximum magnification. Videos of the spherulites falling through the solution were captured, to measure the radius and sedimentation velocity of each spherulite. The spherulite density as a function of radius was calculated from these measurements.

RESULTS

A solution of insulin was prepared and heated in a glass cavity slide at 70°C for 2 h. Inspection of the sample showed a large number of spherulites had formed, which were easily visible with optical microscopy. The spherulites can be seen using DIC contrast or by putting the sample between crossed polarizers, as in Fig. 1 *a*, where each spherulite shows a distinctive Maltese-cross extinction pattern. By scanning up and down through the sample, it could be seen that many spherulites were attached to the lower and upper surfaces of the cell, but relatively few situated between. This observation was made in all our experiments, except when we seeded the solution with preformed spherulites or left the insulin solution unfiltered. In these cases, unattached spherulites could be seen to drift slowly across the field of view as they

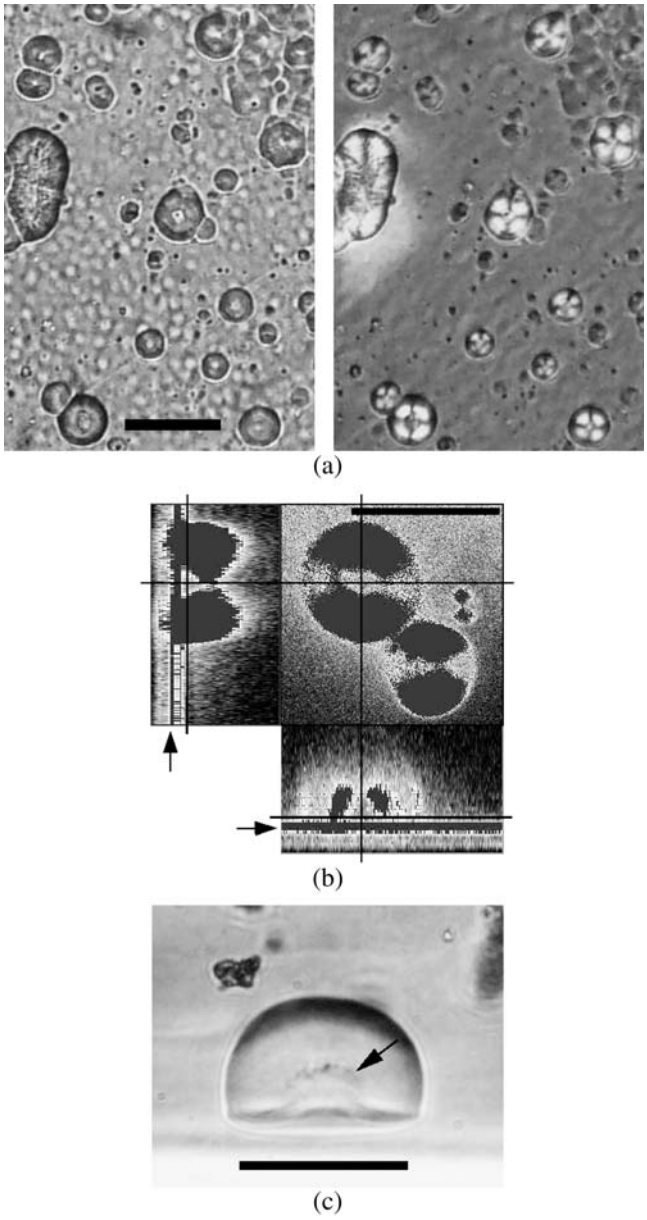

FIGURE 1 Optical microscopy of insulin spherulites attached to a surface. (*a*) DIC contrast (*left*) and optical rotation images (*right*) of the same area (with 100-μm *scale bar*). Out-of-focus blobs are spherulites on opposite surface. (*b*) Confocal microscopy: orthogonal sections (50-μm *scale bar*). Solid lines define sections; arrows show surface of substrate; shading shows regions of saturated fluorescence intensity. (*c*) Horizontal view with DIC contrast (50-μm *scale bar*). Arrow shows the core region.

formed. It is evident that in our preparation conditions, there is a lack of spherulite nucleation sites in bulk solution compared to the surfaces, so the surfaces are where nucleation predominantly occurs. This may be because of the nature of the substrate itself, or because of surface impurities or defects.

Using confocal microscopy, we imaged cross-sections of spherulites formed on the cell surface, using the fluorescent amyloid-specific dye, thioflavin-T. Fig. 1 *b* shows resulting orthogonal sections of a spherulite. The spherulites have a dumbbell-like appearance due to the anisotropic orientation of the dye molecules, which bind to the fibrils, radially arranged in the spherulite (5,6). Each spherulite has a core to which thioflavin-T does not bind. Each core can be seen in contact with the surface of the cell (Fig. 1 *b*), suggesting that it forms or attaches itself there before the spherulite grows around it. The spherulites could also be viewed from the side by careful mounting of their glass substrate in the optical microscope. Fig. 1 *c* shows a horizontal perspective of a surface-bound spherulite, at a slight angle of elevation. In this image, taken with DIC contrast, the spherulite core is also visible. As seen in Fig. 1, *b* and *c*, the spherulites seem to form a dome shape, intermediate between a hemisphere and a full sphere.

The surface spherulites are immobilized while they grow, and therefore they present us with an opportunity to measure the growth of each individually. A sample of insulin was prepared and heated at 75°C, and imaged every 2 min by DIC contrast optical microscopy. A small section of each snapshot is shown in Fig. 2 *a*, and the full video is included in the online supplement to this article (Supplementary Material, Video Suppl. 1). Spherulites appeared after 20 min and grew to diameters of ~100 μm, as can be seen in Fig. 2 *a*. After 42 min, the spherulites have stopped growing. The final image at 68 min is taken again with the sample between crossed polarizers, and shows the characteristic Maltese crosses of the spherulites. The spherulites nucleate at different times and reach a steady-state radius. They are polydisperse at all times.

The complete image of this sample at 68 min is shown in Fig. 2 *b*. Circles are plotted to show the measured radii of all spherulites in focus on that image. A subset of the spherulites in the image was sampled to include the full range of sizes observed (Fig. 3, *inset*). The radii $r(t)$, of the spherulites as a function of heating time t, were measured in each snapshot. Spherulites of $r \approx 5$ μm and smaller appear very dim and diffuse, mainly due to the limitations of our optics, so radii of these values are excluded. A graph of radius against time is shown for this sample (Fig. 3).

The experiment was repeated at temperatures of 65°C and 70°C, and the results are shown in Fig. 4 *a*. As temperature is increased, the lag time before the appearance of spherulites decreases and the spherulites reach a final radius sooner.

Looking at Figs. 3 and 4 *a*, some remarkable features can be noted. Firstly, there is a long lag-time before the appearance of any spherulites, but once a few appear, many more appear within a short time. Each spherulite grows steadily after its first appearance, with radius increasing linearly, or slightly faster than linearly, with time. The growth of each spherulite comes to a sudden stop, at a steady-state radius R, rather than slowing down gradually.

We may plot these curves in another way to emphasize the features of the growth: in Fig. 4 *b*, $r(t) - R$ is plotted so that each curve is superposed after growth ends. This plot shows

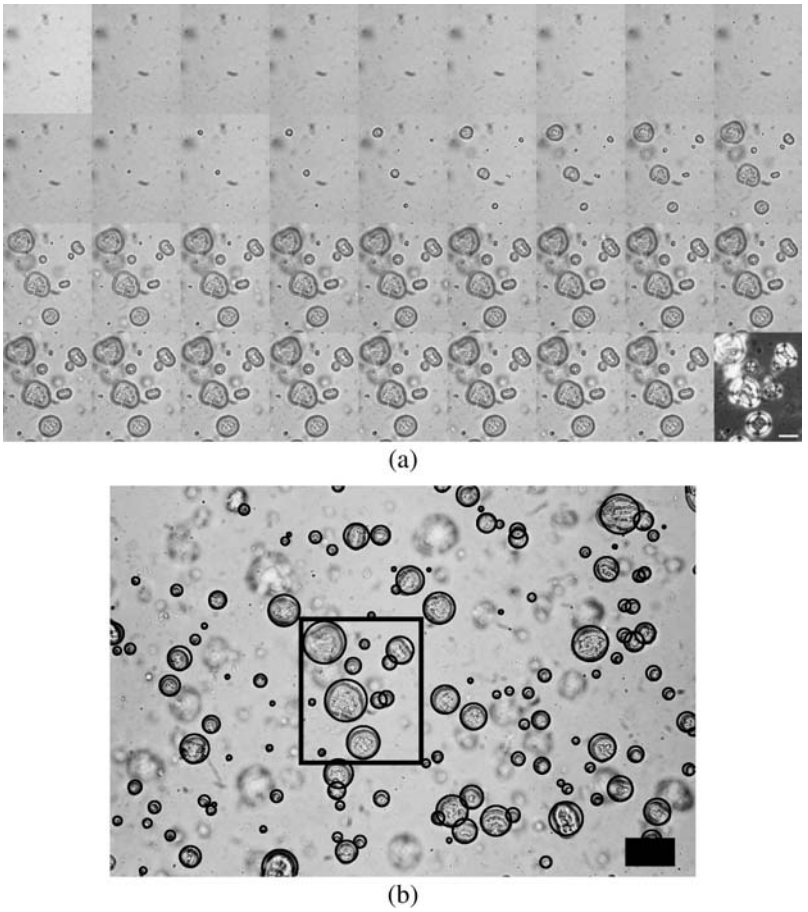

FIGURE 2 Sample of insulin spherulites at 75°C, imaged with DIC contrast. The microscope is focused on the lower surface of the cell. The out-of-focus spherulites are mostly attached to the upper surface. (*a*) Time-lapse frames from 0 to 68 min, arranged in order from left to right, and top to bottom, showing a small section of the complete image (shown in *b*). A 100-μm scale bar is shown (*bottom right*). (*b*) Spherulites after 68 min. As shown, the radii of all spherulites in focus have been measured (*solid circles*). A 200-μm scale bar is shown.

that the sudden end of the growth occurs for all spherulites in each sample at approximately the same halt-time t_R. Halt-times of 108, 68, and 42 min are measured at 65°C, 70°C, and 75°C, respectively, as shown by the arrows in Fig. 4 *b*.

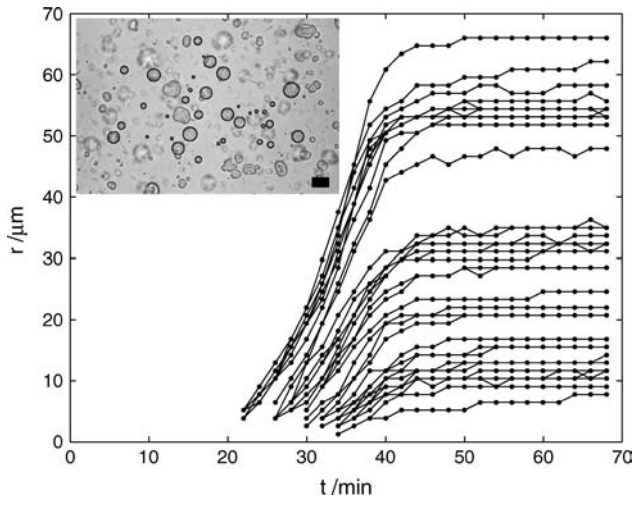

FIGURE 3 Radius measurements as a function of time for spherulites at 75°C. (*Inset*) Measured subset of the complete sample.

The curves have an upward curvature, which shows that the growth accelerates as the spherulites get larger. However, this effect seems to be fairly slight: the lines lie close to a universal curve, as they would if growth rate was constant, for each sample.

The growth curves can be fitted in a simplified way, according to the observed features. To the measurements of $r(t)$ for each spherulite, parameters of nucleation time t_N, initial growth rate k_i, and steady-state radius R, can be fitted.

Our procedure was to define:

1. The steady-state radius R, of a spherulite, as the average of all points of radii satisfying $|r(t) - r(t_F)| \leq 4$ μm, where t_F is the time of the last captured frame.
2. The initial growth rate k_i, of a spherulite, as the average increase of radius per unit time between the first recorded radius and $R/4$.
3. The nucleation time t_N, of a spherulite, by linearly extrapolating the initial growth rate to zero radius.

Fig. 5 *a* shows one result from the sample at 75°C. All measured spherulites were fitted according to this procedure, and the fitted lines of radius against time show a reasonable fit to the measured curves (see Fig. 5 *b*). For all sampled spherulites at each temperature, we plot R, k_i, and t_N against

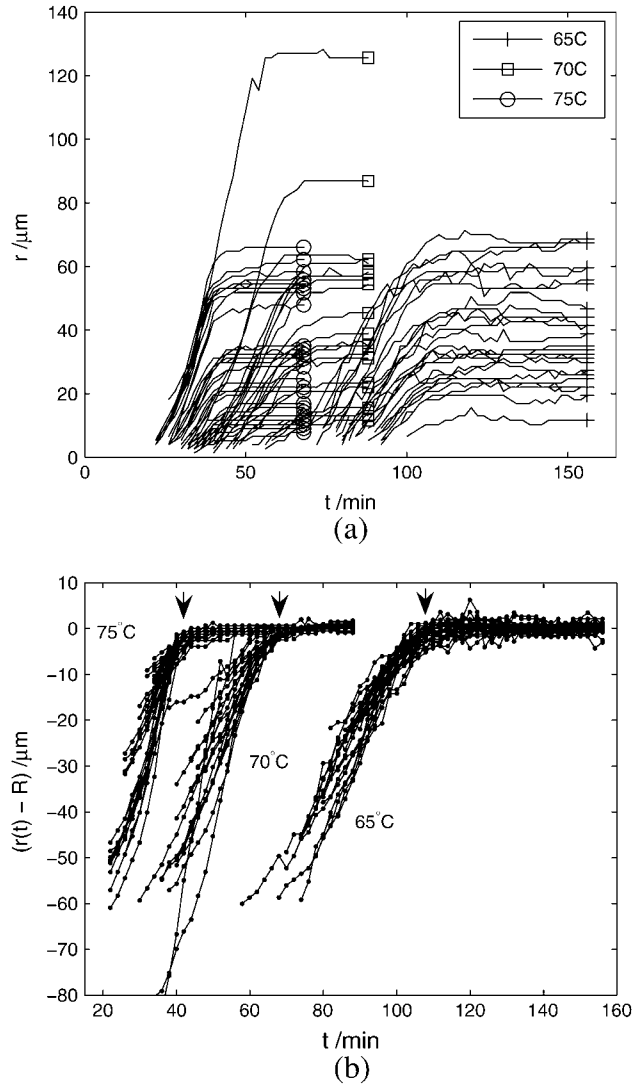

FIGURE 4 Comparison of spherulite growth between samples at 65°C, 70°C, and 75°C. (*a*) Comparison of $r(t)$. (*b*) Comparison of $r(t) - R$. All spherulites in each sample can be seen to stop growing at the same time: 108, 68, and 42 min, respectively, as marked by the arrows.

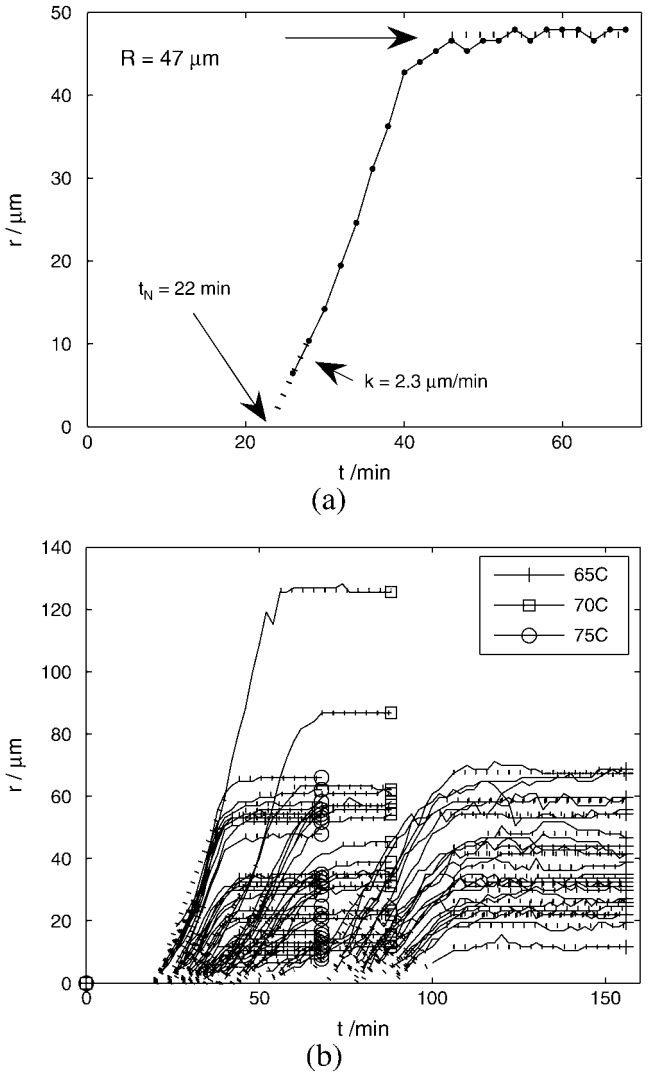

FIGURE 5 Fitting of spherulite growth curves with nucleation time t_N, initial growth rate k_i, and steady-state radius R (*fitted lines* are *dashed*). (*a*) Example fit: single spherulite at 75°C; (*b*) all measured spherulites at 65–75°C.

each other to explore correlations between their values. The results are shown in Fig. 6. Fig. 6, *a* and *c*, show a clear separation in t_N for different temperatures. However, in each sample, there is a large spread of k_i, which seems to be uncorrelated with both R and t_N, and does not change noticeably with increasing temperature (Fig. 6, *b* and *c*). However, R is clearly correlated with t_N for all temperatures, confirming that the growth is steady once the spherulites have nucleated (Fig. 6 *a*). We have fitted the plots of R against t_N with linear least-squares fits (Fig. 6 *a*), yielding correlation coefficients of 0.86, 0.83, and 0.94 at 65°C, 70°C, and 75°C, respectively (see (29), Section 14.5). These fits are in the form corresponding to constant linear growth of the spherulites in a sample:

$$R = -\bar{k}(t_N - t_R), \tag{1}$$

where $\bar{k}$, the average growth rate between the nucleation time and halt-time, has the values 1.50, 2.73, and 3.95 μm/min for 65°C, 70°C, and 75°C, respectively. However, the fitted values of $t_R = 100$, 55, and 33 min, are smaller than the observed halt-times of 108, 68, and 42 min for 65°C, 70°C, and 75°C, respectively. This discrepancy reflects that the growth of the spherulites is slightly accelerating over time, as noticeable in Figs. 3–5.

The features of the growth have been described above without considering the local environment of each spherulite. It seems that characteristics of the local environment, such as proximity of neighboring spherulites, have not had an important effect on the features of the growth as identified above, although they may have contributed to the variation between individual spherulites.

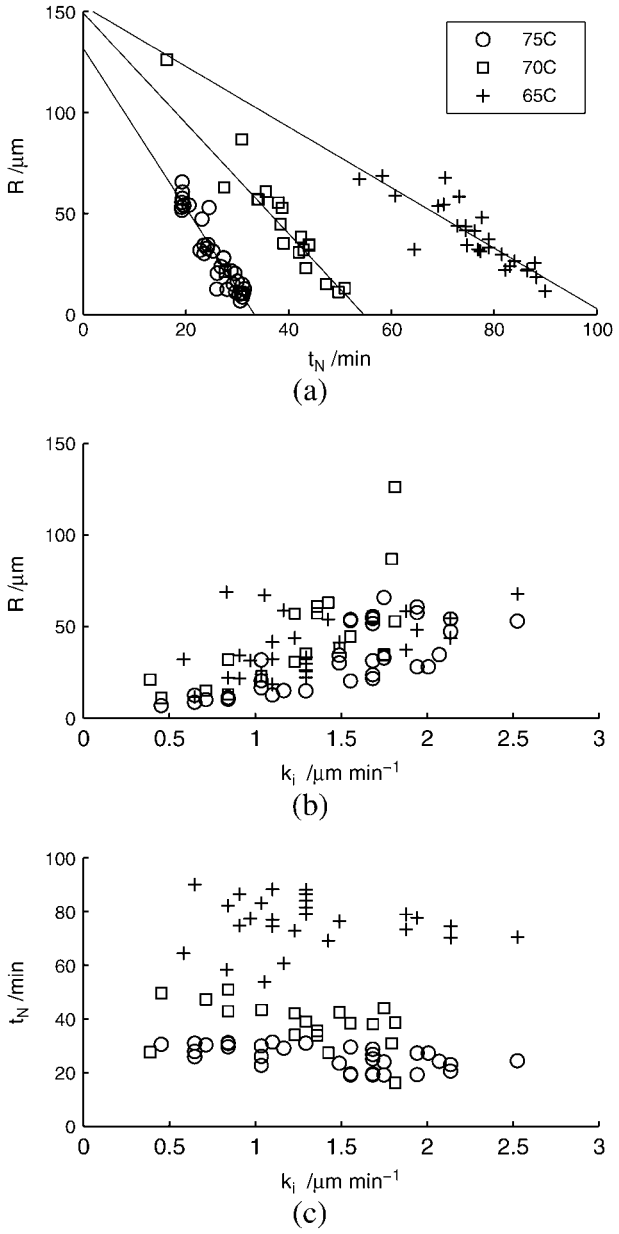

FIGURE 6 Correlations between nucleation time t_N, initial growth rate k_i, and steady-state radius R, for spherulites formed at 65°C, 70°C, and 75°C.

To determine the final size-distribution of the spherulites, $r(t_F)$ was measured for all spherulites in focus in the final image of the samples at each temperature. A histogram of these radii is plotted in Fig. 7. The size distribution is similar at all three temperatures: the count decreases monotonically with increasing radius for $R > 20$ μm. For $R \leq 5$ μm, the spherulites are too dim to be measured. According to the results above, the final radius of each spherulite has an approximately linear dependence on its nucleation time. Therefore, the size-distribution contains preserved information of the nucleation rate as a function of time. The distributions of Fig. 7 thus seem to indicate that this nucleation rate increases

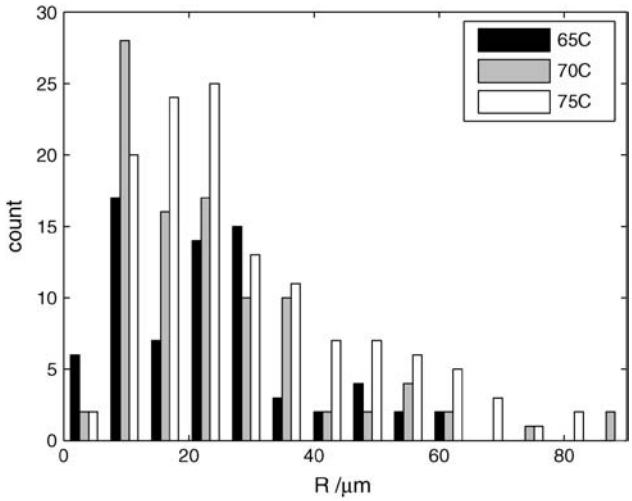

FIGURE 7 Histogram of all radii in final frames of samples at 65°C, 70°C, and 75°C (*left* to *right bars*, respectively).

monotonically for most or all of the growth period for each sample presented.

The formation of large numbers of dome-shaped spherulites on the cell surfaces suggest that surfaces and seeds play an important role in the spherulite nucleation. We tried various experiments to look for such effects.

One experiment tested the difference between cHCl/HNO_3-cleaned glass surfaces and polystyrene surfaces, as examples of strongly hydrophilic and hydrophobic surfaces. Two cells were prepared, filled with an insulin solution, and heated to 70°C. One cell was of cleaned glass as above, and one was solution-coated with polystyrene. As previously, images were taken at 2-min intervals and spherulite radii sampled. The resulting graphs of $r(t)$ are shown in Fig. 8. As

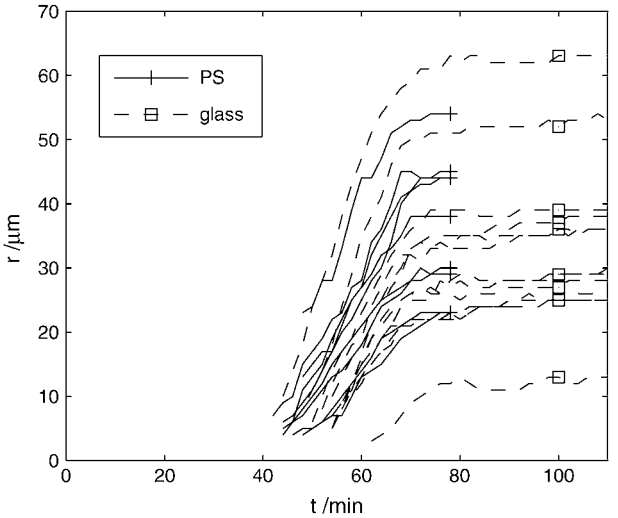

FIGURE 8 Comparison of spherulites grown on cHCl/HNO_3 cleaned glass and polystyrene-coated glass.

can readily be seen, there is no significant difference in growth rates or typical nucleation times between the samples, and the growth period of both samples ends at approximately the same halt-time. This experiment was repeated twice and the same lack of difference noted.

However, a curious effect was observed, which strongly hints at the influence of surface impurities or particles on spherulite nucleation. We made several other samples using glass slides and coverslips straight out of the manufacturer's box, without cHCl/HNO_3 treatment. Fig. 9 shows spherulite beads-on-a-string that formed at 70°C on a glass coverslip surface (Menzel, Braunschweig, Germany; part No. MNJ-350-040B). On untreated glass, these strings appeared in several, but not all, samples. Since this effect was never observed on the cleaned glass, it seems likely that streaks of some unknown impurity are responsible for this very effective spherulite nucleation. (A video of the strings growing is included in the Supplementary Material, Video Suppl. 2.)

We also tried seeding the growth of spherulites by adding rinsed preformed spherulites to a new solution of native insulin, of concentration 5 mg/ml, again heating at 70°C. As can be seen in Fig. 10, the two preformed spherulites in the image grew immediately and steadily, without any time delay after the onset of heating. (A video clip of these preformed spherulites growing is included in the Supplementary Material, Video Suppl. 3.) Apart from the preformed spherulites, new spherulites appeared at times much reduced from the typical nucleation times detailed previously, so that it is possible that these were nucleating on other, smaller seed particles or spherulite fragments from the preformed solution.

Using the same procedure, the growth of preformed spherulites in fresh insulin solutions of variable concentration c, in the range 0.2–5.0 mg/ml, was measured. The initial growth rate k_i of each preformed spherulite at each concentration was determined by a linear fit of the measured $r(t)$ for times $0 \leq t \leq 6$ min (not shown). In Fig. 11, k_i is plotted against c for each preformed spherulite measured. At low insulin concentration, k_i increases with c. However, at $c > 1$ mg/ml, k_i has no obvious dependence on c.

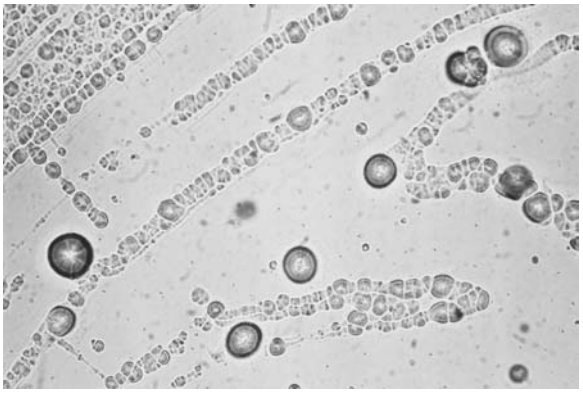

FIGURE 9 The appearance of spherulite strings on an untreated glass surface. A number of large isolated spherulites have also appeared.

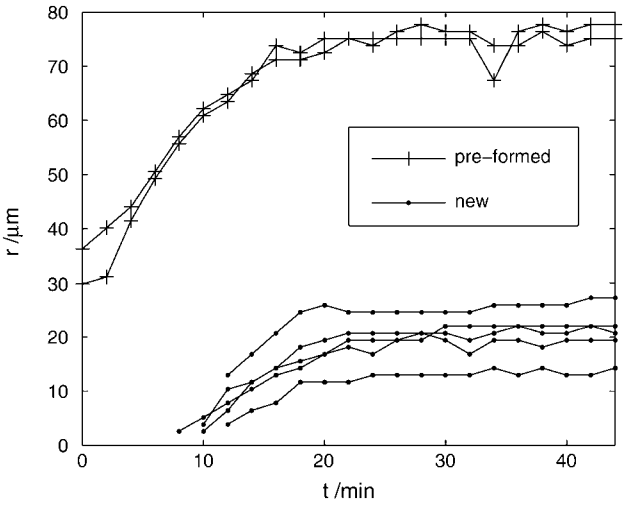

FIGURE 10 Growth of new spherulites compared to preformed spherulites, when added to a fresh solution of insulin and heated at 70°C.

To better understand the structure and growth of the spherulites, we measured the density of insulin spherulites with respect to radius. An insulin solution was prepared and heated at 70°C for 2 h in an Eppendorf tube, producing many unattached spherulites. The spherulites were then transferred to a dilute HCl solution and the radii and sedimentation velocities V, of 57 of them, were measured (see Spherulite Density Measurements, above). The density of spherulites can be calculated from the sedimentation velocity via the Stokes drag for spherical particles, neglecting irregularities in the spherical shape of the spherulites,

$$\Delta\rho = \frac{9\eta V}{2R^2 g}, \tag{2}$$

where $\Delta\rho$ is the difference between the spherulite density and the density of water, $\eta = 1.0$ mPas, and g is the

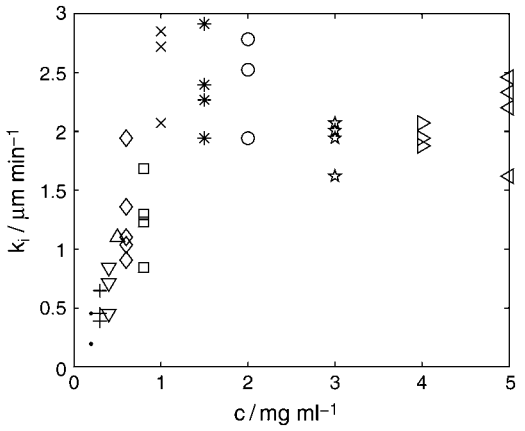

FIGURE 11 Initial growth rates k_i, of preformed spherulites when added to fresh solutions of insulin at concentrations c, and heated at 70°C. (Different markers are used at each concentration for comparison with Fig. 16, where the same data is analyzed and rescaled.)

acceleration due to gravity. V is plotted against R in Fig. 12 for all measured spherulites, and clearly shows the relationship: $V \propto R^2$, indicating that the density of the spherulites is constant with respect to radius. Errors in measuring V are small, as plotted in Fig. 12. A least-squares fit of $V = 7.52 \times 10^4\ \mathrm{m^{-1}\ s^{-1}}\ R^2$ is also plotted in Fig. 12. From the constant of proportionality, we obtain $\Delta\rho = 34.5\ \mathrm{kgm^{-3}}$ using Eq. 2. However, we also note that there is a significant variability between sedimentation velocities of spherulites of the same radius. This variability may be at least partially due to deviations from spherical of the spherulite shape, which would directly affect the sedimentation velocity.

DISCUSSION

Shape, density, and structure

We have observed the formation of dome-shaped insulin spherulites attached to a substrate. Microscopy of the spherulites shows cores in contact with the substrate (Fig. 1, *b* and *c*), and the spherulites extended around them. Video microscopy of growing spherulites shows that they are discrete objects with a clear boundary once r has grown beyond the limit of resolution. It therefore appears that our spherulites have formed by nucleation of a core, and growth by the addition of insulin from solution, in accordance with previous observations (6,27). Krebs et al. found that the core of insulin spherulites is a non-amyloid aggregate, and the major part of the spherulite, the corona, surrounding the core is composed of insulin fibrils aligned in the radial direction (6,27).

Sedimentation experiments have shown that the density of the spherulites is constant with respect to radius. This has interesting implications for the spherulite structure and the arrangement of fibrils within. For this model of the spherulite to satisfy the requirement of constant density (see Results, above), the space in the corona must somehow be filled to keep the density uniform. Any sparse structural model in which the space does not fill as the spherulite grows, would not predict constant density of the spherulite as a function of radius. For example, if we model the spherulite as composed only of one-dimensional fibrils growing unbranched from a central nucleus, we would predict $\Delta\rho \sim R^{-2}$. Similarly, a fractal aggregate model of dimensionality d, similar to those observed in other aggregating systems (30), would predict $\Delta\rho \sim R^{3-d}$. This would be unsatisfactory unless $d = 3$; i.e., the space-filling limit.

This information allows us to elaborate on the schematic model of Krebs et al. (27). As the spherulite expands, the gaps between the growing fibrils must fill such that the density is kept constant. One possibility is that the fibrils branch to produce a three-dimensional structure (Fig. 13). Another possibility is that the gaps in the spherulite fill by nucleation of fibrils at the propagating interface, analogously to the polycrystalline growth models of Granasy et al. (31). Either of these possibilities would represent an additional mechanism involved in the spherulite growth, although our measurements do not yield further information on either.

In the sample we measured, the spherulites are $34.5\ \mathrm{kgm^{-3}}$ denser than water. This value allows us to calculate the number of protein molecules within the spherulite per unit volume, n_m,

$$\Delta\rho = n_\mathrm{m} m_\mathrm{m}\left(1 - \frac{\rho_\mathrm{water}}{\rho_\mathrm{protein}}\right), \tag{3}$$

where m_m is the bovine insulin molecular mass of 5733.5 Da, ρ_protein is the density of protein (i.e., mass of protein divided by volume of all displaced water molecules) for which we use the average value for crystalline protein of $0.81\ \mathrm{Da\ Å^{-3}}$ (32), and $\rho_\mathrm{water} = 998\ \mathrm{kgm^{-3}}$. This yields $n_\mathrm{m} = 1.37 \times 10^{25}\ \mathrm{m^{-3}}$ from our measurements. Neglecting any nonfibrillar protein material that the spherulite may contain, we can now estimate the spacing of fibrils within the spherulite. Jimenez et al. (26) analyzed cryoelectron micrographs of insulin fibrils and found that each insulin molecule occupies 2×4.8 Å of length along each protofilament, variable numbers of

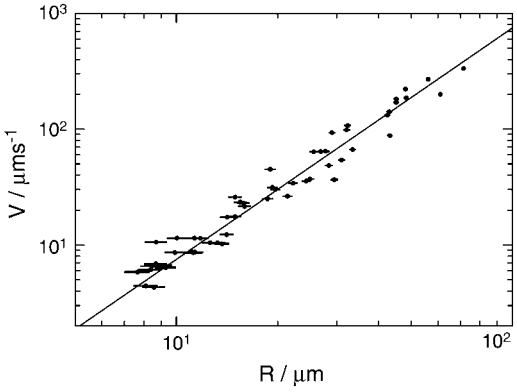

FIGURE 12 Sedimentation velocity V, plotted against radius R, for insulin spherulites, showing a relationship: $V \propto R^2$. The measurement error in V is small (plotted as *vertical error bars*). A least-squares fit of $V = 7.52 \times 10^4\ \mathrm{m^{-1}\ s^{-1}}\ R^2$ is plotted.

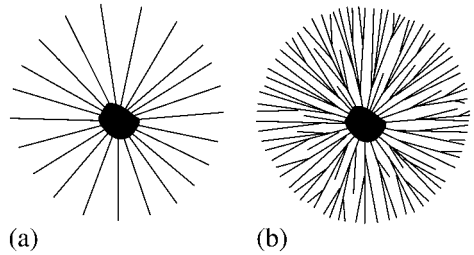

FIGURE 13 Schematic models of spherulites. (*a*) A spherulite composed of unbranched fibrils growing from a central nucleus would not have constant density with respect to radius. Rather the space within the spherulite must fill as the spherulite grows. (*b*) Possibilities are that the fibrils branch or nucleate on the growth front.

which twist together to form the fibrils. For fibrils prepared in similar conditions to ours, they found that only one type of fibril, composed of four protofilaments, was abundant. Assuming that the fibrils in the spherulite are completely aligned and have the same structure as those in the study of Jimenez et al., we obtain a protofibril density (number per unit area perpendicular to the fibril axis), of $n_m \times 9.6\ \text{Å} = 1.3 \times 10^{16}\ \text{m}^{-2}$ and fibril density $\sigma = n_m \times 9.6\ \text{Å}/4 = 3.3 \times 10^{15}\ \text{m}^{-2}$. The latter corresponds to an average separation of $1/\sqrt{\sigma} = 17$ nm between aligned fibrils in the spherulite. Compared to the fibril diameter of 12 nm (26), we can see that the arrangement of fibrils in the spherulite is fairly compact, as illustrated in Fig. 14.

Growth kinetics

The measurements of spherulite growth as a function of time show some remarkable features. The spherulites nucleate at various times, and grow at a rate that increases slightly with increasing radius. Finally, all spherulites in the sample suddenly stop growing at essentially the same time. There is some variability between growth rates of individual spherulites in each sample, just as there is some variability in their shape and density. However, this variability is relatively modest: the growth curves show the same features and approximately the same average growth rate $\bar{k}$, independently of when they have nucleated, and their location with respect to their neighbors.

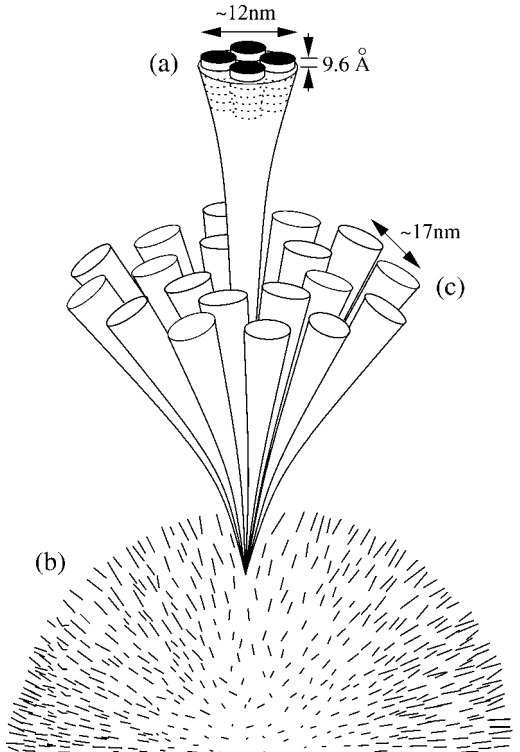

FIGURE 14 Spherulite density and packing. (*a*) The insulin fibril is composed of protofilaments, each a chain of insulin monomers with repeat distance of 9.6 Å (26). Assuming the spherulite is completely composed of these fibrils arranged radially (*b*), the spherulite density allows estimation of the end density of fibrils on the spherulite surface $\sigma = 3.3 \times 10^{15}\ \text{m}^{-2}$. This is equivalent to a 17-nm average fibril separation (*c*).

These observations can be explained within the context of the spherulite structural model discussed above, in which spherulites are composed of amyloid fibrils which nucleate on a core, and grow by the addition of precursor units from the solution to fibril ends on the spherulite surface. The precise form of these precursors is unknown: they could be individual insulin monomers, whether native or in some activated form, or oligomers and larger aggregate species.

The spherulite's radial growth rate is then linked directly to the elongation rate of the fibrils constituting its surface. An elongation-rate-limited polymerization reaction of precursors with fibril ends, where each precursor adds a constant distance d_p to the length of the fibril in a rate-limiting reaction time τ, will produce a constant fibril elongation rate. This would produce a constant radial growth rate κ, if the fibrils are oriented perfectly radially,

$$\kappa = \frac{d_p}{\tau}. \tag{4}$$

If a spherulite contains n precursor units, we can model the precursor addition rate dn/dt, per unit area of spherulite surface, composed of fibril ends of density σ. If the limiting reaction rate $1/\tau$, of precursors joining a fibril end, is lower than the rate at which the precursors can be provided by diffusion, the radial growth rate will be elongation-rate-limited, following Eq. 4. In this case, the precursor addition rate is independent of the concentration of precursors in solution, c_p:

$$\frac{dn_{\text{elo.lim.}}}{dt} = \frac{\sigma}{\tau}. \tag{5}$$

However, if the converse is true: if the limiting reaction rate $1/\tau$ is higher than the rate at which precursors are provided by diffusion, the precursor addition rate will vary with c_p. The extreme case is that the provision of precursors by diffusion is much slower than $1/\tau$, so the precursor addition rate is diffusion-limited. In this extreme, every precursor that reaches the spherulite sticks, and the precursor addition rate, is

$$\frac{dn_{\text{diff.lim.}}}{dt} = \frac{c_p D}{r}, \tag{6}$$

where D is the precursor diffusivity. This expression is based on a steady-state solution of the diffusion equation in spherical coordinates, with a boundary condition of zero precursor concentration at radius r, as appropriate for a sticky sphere of this radius (reviewed in (33)).

If the insulin solutions are prepared with high enough concentration, spherulite growth will follow the limiting

elongation-rate of Eq. 4. Therefore, we identify the observed average growth rate $\bar{k}$, with κ, to compare our model with experiment. The abrupt end of the growth can also be accounted for by the model, assuming that it is caused by the depletion of precursors from the solution. As precursors are consumed, c_p will decrease, until the growth of each spherulite is no longer elongation-rate-limited. By this point, the precursor addition rate will start to fall, eventually reaching zero. For each spherulite, the end of the elongation-rate-limited growth regime will occur when c_p has dropped to a level where $(dn_{elo.lim.}/dt) \sim (dn_{diff.lim.}/dt)$. The equality of these limiting rates (Eqs. 5–6) defines a transition ratio of c_p/r that we shall call γ,

$$\gamma = \frac{\sigma}{D\tau} = \frac{\sigma\kappa}{Dd_p}, \tag{7}$$

using Eq. 4 to substitute for τ. The growth model is shown schematically in Fig. 15. The rate at which precursors are consumed is proportional to the total area of spherulite surfaces in the sample. This area continually increases at an accelerating rate as more and more spherulites nucleate, and those which have nucleated grow, so accordingly we can expect c_p to drop at an accelerating rate. As a result, the precursor addition rate would drop very quickly in time from a steady value to zero, qualitatively producing the observed growth curves, in which the steady growth of each spherulite halts abruptly.

Eq. 7 can be used with the measured growth rates to compare our model with experiment. If we suppose that each precursor is an insulin monomer, then $d_p = 9.6$ Å/4 for a four-protofilament fibril, according to the results of Jimenez et al. (26). An approximate value of D may be obtained according to the Stokes-Einstein diffusivity equation, taking the radius of the insulin monomer as 10.3 Å (the x-ray radius of gyration according to its crystal structure 2INS in the Protein Data Bank, http://www.pdb.org). Then using σ and $\bar{k}$ as calculated from our measurements, we obtain $\gamma = 2.4$, 4.3, and 6.3 mM μm^{-1} or 0.014, 0.025, and 0.037 mg ml^{-1} μm^{-1} for the samples at 65°C, 70°C, and 75°C, respectively.

We have observed steady growth of spherulites with radii up to ~80 μm. Taking $r = 80$ μm, we predict a qualitative steady growth rate for concentrations of $c_p > 1.1$, 2.0, and 2.9 mg/ml, for the samples at 65°C, 70°C, and 75°C, respectively. The initial insulin concentration of 5 mg/ml satisfies these inequalities, so our model is consistent with experiment at all three temperatures. In other words, the spherulite growth in these conditions is slow enough to be limited by the elongation-rate of fibrils on the spherulite surface, as we have described.

The kinetic model can be tested more quantitatively using the measured initial growth rates k_i of preformed spherulites of initial radius r, growing at 70°C (see Results, above). For convenience, we take c_p equal to the initial insulin concentration c, and examine this assertion later. Plotting k_i against c/r for each spherulite then allows a direct comparison with the elongation-rate and diffusion limits, as modeled in Eqs. 4 and 5 and illustrated in Fig. 15. The result is shown in Fig. 16. The measured points show a reasonable quantitative agreement with our model. Within the error of radius measurement and the variability between individual spherulites, k_i exhibits two regimes: it increases with c/r for c/r small, and remains constant for c/r large. The transition between the regimes occurs at $c/r \approx \gamma = 0.025$ mg ml^{-1} μm^{-1} as we have predicted, taking $\kappa = \bar{k} = 2.73$ μm/min as above. We emphasize that no adjustable parameters have been used in this comparison: the growth rate $\bar{k}$, and fibril-end density σ, were determined from other measurements in this article; the monomer repeat distance, d_p, is from the fibril structural model of Jimenez et al. (26); and the diffusivity, D, was calculated from the monomer's radius of gyration. Looking again at Eq. 7, we can also see that the calculation of γ is independent of the number of protofilaments per fibril, since both σ and d_p are inversely proportional to this number.

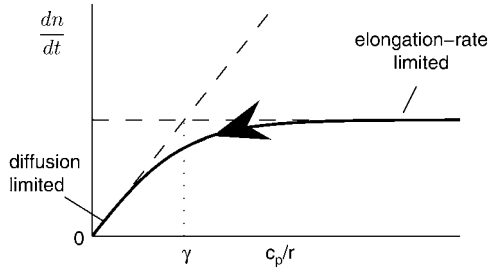

FIGURE 15 Schematic model of spherulite growth: as spherulites nucleate and grow, the precursor concentration c_p decreases. Each spherulite follows the trajectory shown: the rate of precursor addition per unit area, (dn/dt), is constant until c_p/r falls to $\sim\gamma$.

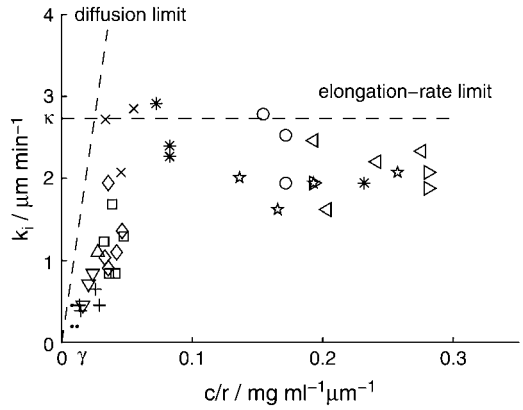

FIGURE 16 Growth of preformed spherulites when added to fresh solutions of insulin, heated at 70°C. Initial growth rate k_i is plotted against the initial ratio of concentration to radius c/r, for each spherulite, allowing direct comparison with the predicted growth kinetics: a elongation-rate limit of $\kappa = \bar{k} = 2.73$ μm min^{-1} for $c/r \gg \gamma = 0.025$ mg ml^{-1} μm^{-1} and diffusion limit for $c/r \ll \gamma$. (The different markers are used to identify concentrations in the range $0.3 \le c \le 5$ mg/ml, according to the scale of Fig. 11.)

Our assumptions that the precursor species is the insulin monomer, and that c_p equals c, must be examined. Our calculation of γ is approximately independent of the identity of the precursor, since γ depends on the product Dd_p (Eq. 7), and both D and d_p depend on the linear dimension of the precursor, being proportional and inversely proportional, respectively. Our model is therefore insensitive to the actual identity of the precursor, whether it is an insulin monomer, an oligomer, or larger aggregate species. However, by equating the precursor concentration c_p, with the insulin concentration c, we have also assumed that all insulin in solution is in its precursor form. We may tentatively examine this assumption by comparing the measured and predicted diffusion-limited growth rates, as $c/r \rightarrow 0$. The measured k_i values in this region are close to, but noticeably below, the predicted diffusion-limit (Fig. 16). This comparison suggests that a large fraction, but not all, of the insulin in solution at 70°C and pH 1.5 is in its precursor form at the onset of heating. Therefore, the precursor is likely to be a monomeric or small oligomeric form of insulin, and cannot be a species which takes a significant heating time to form. This result supports the suggestion of Krebs et al. (6).

We noted above that the radial growth rate of each spherulite was not quite constant, but tended to accelerate slightly with time during the growth period. This observation may have several qualitative explanations. Rather than the fibrils being perfectly radially ordered, their order of alignment may increase as the spherulite radius increases. The branching or filling of space between the fibrils as they radially diverge may also affect the growth rate: there will be more space to fill for a radial increment Δr, per unit surface area, at small r than large r. Alternatively, the accelerating growth may reflect some characteristic difference between the spherulite core and corona.

Nucleation

Insulin spherulites can form as surface-bound domes as well as suspended spheres. In our experiments, the high ratio of surface area to volume of each cell, and the lack of nucleation sites in the filtered protein solution, appear to have favored nucleation of spherulites on the surfaces relative to the bulk.

The seeding of insulin solutions with preformed spherulites led to the preformed spherulites growing immediately at the onset of heating, without a time delay. Therefore, it seems that the fibril ends that constitute the spherulite surface have remained active after they stop growing due to depletion of precursor, in the sense that when a spherulite is transferred to a new insulin solution, the ends can continue growing without a time delay.

The formation of surface-bound insulin spherulites was not affected by the simple hydropathicity of the surface. Spherulites grown on hydrophilic glass and hydrophobic polystyrene substrates showed no difference in nucleation times, growth rates, or the halt-time. It should be pointed out that this is an unexpected finding. Sluzky et al. (34) found that agitation of an insulin solution increased the propensity of spherulite formation, and interpreted the positive result as being caused by the increased area of the hydrophobic air interface. Other experimental studies have also discussed the positive role of hydrophobic interactions on the formation of amyloid fibrils in general and insulin in particular (e.g., (24,35)).

The formation of strings of spherulites on untreated glass strongly hints at the influence of surface impurities or particles on spherulite nucleation. It would be most interesting to find and characterize substances that can induce the formation of amyloid spherulites.

CONCLUSIONS

We have observed bovine insulin spherulites forming on cell surfaces using DIC-contrast optical microscopy, and tracked the growth of individual spherulites with time. The density of the spherulites and their formation under variable conditions have also been studied to provide insights into their structure, formation mechanism, and growth kinetics. A model of spherulite formation based on the radial elongation of oriented fibrils around a nucleus, by polymerization from a precursor in solution, where the growth is limited by the rates of fibril elongation and precursor diffusion, quantitatively accounts for the observed growth kinetics.

Our method allows us to follow the formation of individual amyloid spherulites immobilized on a surface, directly—thus providing an ideal opportunity for testing the effect of surfaces and seeds on the formation of spherulites, as a model of physiological amyloid plaques.

SUPPLEMENTARY MATERIAL

An online supplement to this article can be found by visiting BJ Online at http://www.biophysj.org.

Thanks to Eugene Terentiev for some encouraging theoretical suggestions, Leonard Sagis for his comments on the draft, and Paul Venema, Cynthia Akkermans, and Suzanne Bolder, for fruitful conversations.

S.S.R. gratefully acknowledges the Biotechnology and Biological Sciences Research Council for providing his studentship funding.

REFERENCES

1. Dobson, C. M. 2003. Protein folding and misfolding. *Nature*. 426: 884–890.
2. Lashuel, H. A., S. R. LaBrenz, L. Woo, L. C. Serpell, and J. W. Kelly. 2000. A peptidomimetic that forms cables, monolayers (or bilayers) or fibrils depending on solution conditions: implications for material science and neurodegenerative diseases. *J. Am. Chem. Soc.* 122: 5262–5277.
3. Dobson, C. M. 1999. Protein misfolding, evolution and diseases. *Trends Biochem. Sci.* 24:329–332.

4. Sunde, M., and C. C. F. Blake. 1997. The structure of amyloid fibrils by electron microscopy and x-ray diffraction. *Adv. Protein Chem.* 50: 123–159.

5. Jin, L., K. Claborn, M. Kurimoto, M. Geday, I. Maezawa, F. Sohraby, M. Estrada, W. Kaminsky, and B. Kahr. 2003. Imaging linear birefringence and dichroism in cerebral amyloid pathologies. *Proc. Natl. Acad. Sci. USA.* 100:15294–15298.

6. Krebs, M. R. H., E. H. C. Bromley, S. S. Rogers, and A. M. Donald. 2005. The mechanism of amyloid spherulite formation by bovine insulin. *Biophys. J.* 88:2013–2021.

7. Waugh, D. F. 1946. A fibrous modification of insulin. I. The heat precipitate of insulin. *J. Am. Chem. Soc.* 68:247–250.

8. Acebo, E., M. Mayorga, and J. F. Val-Bernal. 1999. Primary amyloid tumor (amyloidoma) of the jejunum with spheroid type of amyloid. *For. Pathol.* 31:8–11.

9. Aggeli, A., M. Bell, L. M. Carrick, C. W. G. Fishwick, R. Harding, P. J. Mawer, S. E. Radford, A. E. Strong, and N. Boden. 2003. pH as a trigger of peptide β-sheet self-assembly and reversible switching between nematic and isotropic phases. *J. Am. Chem. Soc.* 125:9619–9628.

10. Bromley, E. H. C., M. R. H. Krebs, and A. M. Donald. 2005. Aggregation across the lengthscales in β-lactoglobulin. *Faraday Discuss.* 128:13–27.

11. Fezoui, Y., D. M. Hartley, D. M. Walsh, D. J. Selkoe, J. J. Osterhout, and D. B. Teplow. 2000. A de novo designed helix-turn-helix peptide forms nontoxic amyloid fibrils. *Nat. Struct. Biol.* 7:1095–1099.

12. Hamodrakas, S. J., A. Hoenger, and V. A. Iconomidou. 2004. Amyloid fibrillogenesis of silk moth chorion protein peptide-analogues via a liquid crystalline intermediate phase. *J. Struct. Biol.* 145:226–235.

13. Lockwood, N. A., R. van Tankeren, and K. H. Mayo. 2002. Aqueous gel derived from the β-sheet domain of platelet factor-4. *Biomacromolecules.* 3:1225–1232.

14. Manuelidis, L., W. Fritch, and X. You-Gen. 1997. Evolution of a strain of CJD that induces BSE-like plaques. *Science.* 277:94–98.

15. Raffen, R., L. J. Dieckman, M. Szpunar, C. Wunschl, P. R. Pokkuluri, P. Dave, D. Wilkins-Stevens, X. Cai, M. Schiffer, and F. J. Stevens. 1999. Physicochemical consequences of amino acid variations that contribute to fibril formation by immunoglobulin light chains. *Protein Sci.* 8:509–517.

16. Ruth, L., D. Eisenberg, and E. F. Neufeld. 2000. α-l-iduronidase forms semi-crystalline spherulites with amyloid-like properties. *Acta Crystallogr.* D56:524–528.

17. Sagis, L. M. C., C. Veerman, and E. van der Linden. 2004. Mesoscopic properties of semiflexible amyloid fibrils. *Langmuir.* 20:924–927.

18. Snow, A. D., R. Sekiguchi, D. Nochlin, P. Fraser, K. Kimata, A. Mizutani, M. Arai, W. A. Schreier, and D. G. Morgan. 1994. An important role of heparan sulfate proteoglycan (perlecan) in a model system for the deposition and persistence of fibrillar AB-amyloid in rat brain. *Neuron.* 12:219–234.

19. Taniyama, H., A. Kitamura, Y. Kagawa, K. Hirayama, T. Yoshino, and S. Kamiya. 2000. Localized amyloidosis in canine mammary tumors. *Vet. Pathol.* 37:104–107.

20. Vos, J. H., and E. Gruys. 1985. Amyloid in canine mammary tumors. *Vet. Pathol.* 22:347–354.

21. Bassett, D. C. 2003. Polymer spherulites: a modern assessment. *J. Macromol. Sci. Phys.* 42:227–256.

22. Donald, A. M., and A. H. Windle. 1992. Liquid Crystalline Polymers. Cambridge University Press, Cambridge, UK.

23. Magill, J. H. 2001. Spherulites: a personal perspective. *J. Mater. Sci.* 36:3143–3164.

24. Nielsen, L., R. Khurana, A. Coats, S. Frokjaer, J. Brange, S. Vyas, V. Uversky, and A. Fink. 2001. Effect of environmental factors on the kinetics of insulin fibril formation: elucidation of the molecular mechanism. *Biochemistry.* 40:6036–6046.

25. Bouchard, M., J. Zurdo, E. Nettleton, C. Dobson, and C. Robinson. 2000. Formation of insulin amyloid fibrils followed by FTIR simultaneously with CD and electron microscopy. *Protein Sci.* 9: 1960–1967.

26. Jimenez, J. L., E. J. Nettleton, M. Bouchard, C. V. Robinson, C. M. Dobson, and H. R. Saibil. 2002. The protofilament structure of insulin amyloid fibrils. *Proc. Natl. Acad. Sci. USA.* 99:9196–9201.

27. Krebs, M. R. H., C. E. MacPhee, A. F. Miller, I. E. Dunlop, C. M. Dobson, and A. M. Donald. 2004. The formation of spherulites by amyloid fibrils of bovine insulin. *Proc. Natl. Acad. Sci. USA.* 101: 14420–14424.

28. Krebs, M. R. H., E. H. C. Bromley, and A. M. Donald. 2005. The binding of thioflavin-T to amyloid fibrils: localisation and implications. *J. Struct. Biol.* 149:30–37.

29. Press, W. H., B. P. Flannery, S. A. Teukolsky, and W. T. Vetterling. 1993. Numerical Recipes in C, 2nd Ed. Cambridge University Press, Cambridge, UK.

30. Jullien, R., and R. Botet. 1987. Aggregation and Fractal Aggregates. World Scientific, Singapore.

31. Granasy, L., T. Pusztai, T. Borzsonyi, J. A. Warren, and J. F. Douglas. 2004. A general mechanism of polycrystalline growth. *Nat. Mater.* 3: 645–650.

32. Andersson, K. M., and S. Hovmoller. 2000. The protein content in crystals and packing coefficients in different space groups. *Acta Crytallogr. D Biol. Crystallogr.* 56:789–790.

33. Bray, A. J. 2002. Theory of phase-ordering kinetics. *Adv. Phys.* 52: 481–587.

34. Sluzky, V., J. Tamada, A. Klibanov, and R. Langer. 1991. Kinetics of insulin aggregation in aqueous-solutions upon agitation in the presence of hydrophobic surfaces. *Proc. Natl. Acad. Sci. USA.* 88:9377–9381.

35. Dzwolak, W., R. Ravindra, and R. Winter. 2004. Hydration and structure—the two sides of the insulin aggregation process. *Phys. Chem. Chem. Phys.* 6:1938–1943.